Linkages between tropical Pacific seasonal, interannual, and orbital variability during the Holocene

Linkages between tropical Pacific seasonal, interannual, and orbital variability during the Holocene

J. Emile-Geay[1*], K.M. Cobb[2], M. Carré[3], P. Braconnot[4], J. Leloup[5], Y. Zhou[1],

S.P. Harrison[6], T. Corrège[7], H.V. McGregor[8], M. Collins[9], R. Driscoll[10], M. Elliot[11],

B. Schneider[12], A. Tudhope[10]

[1]*Department of Earth Sciences, University of Southern California, Los Angeles, CA 90089, USA*

[2]*School of Earth and Atmospheric Sciences, Georgia Institute of Technology, Atlanta, GA 30332, USA*

[3]*Institut des Sciences de l'Evolution, Université de Montpellier, CNRS, IRD, EPHE, Montpellier 34095, France*

[4]*IPSL/LSCE, unité mixte CEA-CNRS-UVSQ, Gif sur Yvette 91191, France*

[5]*Sorbonne Universités, UPMC Univ. Paris 6, LOCEAN/IPSL, UMR 7159, CNRS-IRD-MNHN, Paris, France*

[6]*Centre for Past Climate Change and School of Archaeology, Geography and Environmental Sciences (SAGES) University of Reading, Whiteknights, Reading, RG6 6AB, UK*

[7]*UMR 5805 EPOC, Université de Bordeaux, Pessac, France*

[8]*School of Earth and Environmental Sciences, University of Wollongong, Wollongong, NSW 2522, Australia*

[9]*College of Engineering, Mathematics and Physical Sciences, University of Exeter, Laver Building, North Park Road, Exeter, EX4 4QE, UK*

[10]*University of Edinburgh, School of GeoSciences, James Hutton Road, Edinburgh EH9 3FE, UK*

[11]*Paleoclimats Paleoenvironnements Bioindicateurs, Université de Nantes, LPGNantes, 2 rue de la Houssinière, Nantes 44300, France*

[12]*Institut für Geowissenschaften, Universität Kiel, D-24118 Kiel, Germany*

The response of the El Niño/ Southern Oscillation (ENSO) to external forcing is a central issue in climate science. It is unclear how ENSO responds to natural forcing, particularly orbitally-induced changes in the amplitude of the seasonal cycle. Here we reconstruct seasonal and interannual variability using a network of high-resolution marine records from the tropical Pacific Ocean spanning discrete intervals of the Holocene. We then compare our reconstructed ENSO activity to that simulated by nine climate models. The records display several intervals of reduced ENSO variance, notably a 2/3 reduction between 5,000 and 3,000 years ago. The reconstructed changes are not in phase with equatorial insolation, nor is their amplitude or timing accurately captured by the models. Moreover, the models do not predict the mid-Holocene increase in seasonality evident in the observations. While the simulations suggest an inverse relationship between the amplitude of the seasonal cycle and ENSO-related variance in sea surface temperatures, the observations do not. We therefore conclude that tropical Pacific climate is highly variable and subject to millennial-scale quiescent periods. Such periods harbor a complex link, if any, to orbital forcing, and are inadequately simulated by the current generation of climate models, highlighting a major gap in our understanding of a climate system of global importance.

ENSO, the oscillatory instability of the tropical Pacific ocean–atmosphere system, is the leading pattern of global interannual variability, with important physical, ecological, and human

impacts[1]. Yet, predicting its long-term behavior in the face of continued anthropogenic forcing has proven elusive[2]. While the predictive skill of climate models at interannual timescales can be tested using instrumental observations, such records are too short to evaluate the fidelity of model-simulated tropical Pacific variability on adaptation-relevant timescales. This motivates the use of paleoclimate observations, which cover a much longer time span and predate the instrumental observations used to develop and tune climate models, hence providing an out-of-sample test of their predictive ability[3].

The mid-Holocene (MH, ca 6,500 yrs before present; 6.5 kyBP) represents a key target for evaluating the simulated response of ENSO to external forcing. While ice volume and greenhouse gas concentrations were essentially similar to today, the latitudinal and seasonal distribution of incoming solar radiation (insolation) was markedly different as a result of precession[4]: seasonal contrast was amplified in the northern hemisphere and reduced in the southern hemisphere. Thus, the mid-Holocene provides an opportunity to explore the link between changes in the seasonal cycle, meridional asymmetry in the equatorial zone, and ENSO behavior. Several circum-Pacific paleoclimate records have been interpreted as implying a marked reduction in ENSO activity during the MH[5–7], a reduction simulated by models of various complexity[8–13]. Furthermore, this reduction has been dynamically linked either to changes in the linear stability of ENSO [9], or to an insolation-driven increase in the amplitude of the annual cycle in near-equatorial SST (hereafter, AC)[9,10,12], in line with evidence for a negative correlation between ENSO and the AC documented in instrumental observations[14] and modeling studies of current and past climate states[8,15–19].

Several mechanisms have been proposed to account for the seasonal cycle influence on ENSO: frequency locking[15,20]; nonlinear resonance between annual and internal modes[21,22], and combination tones of ENSO and the AC[23]. We note, however, that the inverse link between ENSO variance and AC amplitude is not universal amongst models[4,10] nor in the various proposed mechanisms. While some seasonally-resolved paleoclimate records suggest a strong dynamical link between precessional forcing and ENSO activity[24], reconstructions of central and eastern Pacific ENSO variance do not[25,26]. A synthesis of the available observations and simulations of ENSO and the annual cycle is timely, and would help constrain ENSO sensitivity to external forcing.

Here we synthesize high-resolution, well-dated paleoclimate records from across the tropical Pacific spanning the Holocene (see Extended Methods). We compare these observations to an ensemble of nine state-of-the-art global climate models (GCMs) from the Paleoclimate Modeling Intercomparison Project (PMIP3[27]), which include simulations of pre-industrial (*piControl*) as well as industrial (*historical*) and MH (*midHolocene*) climate (Supplementary Table S2). This dataset constitutes the most comprehensive collection of oxygen isotope measurements on Holocene corals[5,6,24,25,28–34] and mollusks[26,35–37] to date from the tropical Pacific (Figure 1, Supplementary Table S1, Supplementary Figures S1-S6). Such marine carbonates record the isotopic composition of oxygen (δ^{18}O), which reflects changes in sea-surface temperature (SST, Supplementary Figure S10a) as well as the δ^{18}O of seawater (the latter linearly related to sea-surface salinity (SSS, Supplementary Figure S10b). The isotopic signal is generally dominated by the thermal component, except in the far western Pacific (Supplementary Figure S11). All records have annual or finer resolution and collectively cover ~ 2000 out of the past 10,000 years (Sup-

plementary Table S1 and Figure S1). There are three clusters of sites in the western (WP: Papua New Guinea, New Caledonia, Vanuatu, Surprise Atoll), central (CP: the Line Islands of Palmyra, Fanning and Christmas) and eastern (EP: Peruvian coast) tropical Pacific.

Seasonal and interannual variability over the Holocene

The seasonal and interannual components of the tropical Pacific records display much irregularity in interannual (2–7y) variance – a measure of ENSO activity – as well as in AC amplitude. To enable comparisons between different records and sites, we show the ratio between fossil and modern (twentieth century) values of interannual variance and AC amplitude (Figure 2), with uncertainties estimated via the block bootstrap (Extended Methods). Most records of ENSO variance plot below unity, implying that twentieth century ENSO was unusually active[25,38]. Those fossil samples displaying higher-than-modern ENSO variance have large uncertainties compatible with no change. Such uncertainties are usually the consequence of short fossil and/or modern sequences.

Despite appreciable differences between ENSO reconstructions from the three regions, some consistent patterns do emerge. In the western Pacific (Figure 2, top), the records show a significant decrease in ENSO variance during the early and mid-Holocene[5,6,29,36]; there are only a few records from the 6-2 kyBP interval but these also show reduced ENSO variance. Low ENSO variance is present throughout the past 7ky in the CP (Figure 2, center), with the most consistent signal corresponding to a 64% reduction occurring between 3-5 kyBP (Table 1) and a trend from extremely low variance to the present state from 2 kyBP onwards[24,25]. Records from the EP show ENSO

variance either similar to or lower than today, with the deepest reduction around 4.6 kyBP (Figure 2, bottom)[26]. Thus, our data set suggests that the mid-Holocene reduction in ENSO variance identified in previous studies[5–7,32] is not an exceptional event, but rather that ENSO may have been less active than at present for much of the Holocene.

Reconstructions of the AC amplitude display little coherence through time. Records from the western Pacific show AC amplitudes similar to present before 7 kyBP. However, records from the interval 7-4 kyBP unequivocally display a reduced AC amplitude, while after 3 kyBP the records show a return to AC amplitudes similar to the present day. In contrast, records from the CP show considerable temporal structure in AC amplitude, although many of the individual records have high levels of uncertainty. In the eastern Pacific, the records show slightly reduced AC amplitude throughout the past 10 ky, except for a period with amplitude similar to the present day at 3 kyBP.

Comparisons with simulated tropical Pacific climates

We now use this dataset to constrain the behavior of PMIP3 models. Although there are comparatively few records from precisely 6.5 kyBP, we assume that the changes recorded during the window between ca 7.5 and 5.5 kyBP are representative of the mid-Holocene and provide an indication of the average change to be expected in the MH simulations. In order to make quantitative model-data comparisons, we translate model output into oxygen isotope ratios using a forward modeling approach[39,40], in which the δ^{18}O of biocarbonates is parameterized as a function of SSS and SST (Extended Methods). This approximates the isotopic variations that would have been

recorded by the coral or mollusk in response to the simulated changes in climate produced by each climate model, which can then be directly compared to the observed variations at a site (Supplementary Figures S10, S11). The forward model is a simplified representation of the incorporation of ^{18}O by mollusk and coral systems, in particular because it represents the relationship between seawater ^{18}O and SSS as time-invariant. However, it has been shown to reproduce the first-order basin-scale variability contained in modern corals from across the tropical Pacific[39]. Thus, this simple model provides a way of bridging GCMs and paleo observations.

Most of our records are comparatively short: the average record length is around 50 years (Supplementary Figure S1b) and very few are longer than 100 years. As ENSO variability is non-stationary, quantifying ENSO variance over such short windows leads to a wide range of estimates[41,42]. Random sampling of multi-century model simulations under stationary boundary conditions shows that ENSO variance estimates on 50-year windows may vary by up to $\pm 50\%$ from sampling alone (Supplementary Figure S13); these estimates converge as the observation window lengthens. Thus, the short length of most of the observations could make it difficult to discriminate between observed and simulated variability. Changes in the AC amplitude are much better constrained, though still sensitive to segment length (Supplementary Figures S12, S13).

For each model, we estimate the statistical distributions of modeled ENSO and AC amplitude for 50-year periods via the block bootstrap for both the *piControl* and *midHolocene* simulations (Supplementary Table S2) and compare these distributions to the values obtained from the *historical* simulations (Supplementary Figures S14-22). The distributions of ENSO variance ratios are

broad and positively skewed, while those of AC amplitude are narrow and symmetric (Figure 2, colored curves). ENSO variance ratios are clustered around unity in the *piControl* experiments, and fall below unity in most of the *midHolocene* experiments. The *midHolocene* reduction is small and, given the width of the distributions, only marginally significant at the 5% level. Nonetheless, it is qualitatively consistent with results from an intermediate complexity model[8] as well as many other GCM simulations[9–13], all of which show reduced ENSO variability during the mid-Holocene compared to the pre-industrial climate.

While the synthesis of existing paleo-ENSO data present a heterogeneous picture of ENSO variability through both space and time, there is evidence for a sustained reduction in ENSO variability from 3-5 kyBP. This is especially true in the CP, where a deep reduction (64%) is accompanied by a relatively narrow 95% confidence interval (CI) of $[28\%, 84\%]$ (Table 1). Reductions of similar magnitude are observed during the MH (5.5-7.5 kyBP) (66% in the center, 50% in the West, 33% in the East), albeit with CIs so wide that they cannot exclude increases in ENSO variance (Table 1). Thus, a salient feature of this dataset is a robust, approximately two-thirds reduction in CP interannual variance, which appears to have persisted throughout much of the 3-5 kyBP interval. This persistent reduction bears little resemblance to the model simulations of reduced MH ENSO[4,8] followed by a gradual intensification to the present[13], and happened at a time when boreal summer/winter precessional forcing was weaker than during the MH (Supplementary Figure S9).

Can PMIP3 GCMs simulate the magnitude of such reductions, and if so, under which conditions? We answer this question by computing the probability of observing ENSO variance re-

ductions of at least 64% on 50-year segments (Table 2). These probabilities are extremely low under pre-industrial conditions, ranging from 1 to 12%. Such occurrences are still rare under MH boundary conditions (probabilities ranging from 3 to 15%), though most (7 out of 9) of the models show an increased probability of ENSO reduction. Thus, while orbital forcing characteristic of the MH tends to drive simulated changes in ENSO variance in the right direction, the amplitude of simulated changes is too modest, and the response is not consistent among models. It is even harder to explain the larger, more sustained reductions that may have prevailed during the 3-5 kyBP period, but the short length of the simulations (Supplementary Table S2) precludes an assessment of this question.

The models all show a reduction in the median amplitude of the AC in the *midHolocene* simulations, for all three regions. The reduction is between 10% to 50% (depending on the model) but is relatively uniform across the basin (Figure 2, right). This uniformity contrasts strongly with the observed changes in the 7.5-5.5 kyBP window, where AC amplitude is decreased in the western Pacific but increased in the CP. However, the reduction in AC amplitude in the western Pacific is $\sim 50\%$ larger than in the simulations.

Links between ENSO and the seasonal cycle amplitude

We investigate the link between changes in ENSO variance and in AC amplitude by plotting the fossil to modern ratio of ENSO-band variance against the same ratio of AC amplitude, in both Holocene observations and PMIP3 simulations (Figure 3). Both axes are scaled by their uncer-

tainty to make an orthogonal regression possible (Extended Methods). The simulated relationship is significantly negative (Figure 3, bottom), in agreement with previous work[17–20]. This contrasts with the observations, which reveal a weak positive relationship between ENSO variance and AC amplitude (Figure 3, top). Moreover, the range of variations in AC amplitude is about 2-3 times larger in the observations than in the simulations (Supplementary Figure S23). Similar results emerge if only data from the CP are considered (Supplementary Figures S24–25), or if wavelet analysis is used to diagnose the relationship between energy in the annual and interannual bands[19] (Extended Methods, Supplementary Figure S26). If our interpretation of the data is correct, the mismatch between the observed and simulated relationship between ENSO variance and AC amplitude has important dynamical implications. The frequency entrainment hypothesis[15,20] states that a self-exciting oscillator will give up its independent mode of oscillation and acquire the frequency of the applied forcing (in this case, the AC in insolation). It has long been invoked to explain the inverse relationship between ENSO and the AC in coupled GCMs [12,13,17,18]. Our results confirm that this link is strong in PMIP3 models, but suggest that it is opposite to that found in observations over the Holocene.

In comparing the ENSO-AC relationship across models and data, it is important to note the limitations associated with using a sparse set of observations to constrain tropical Pacific dynamics. One possible explanation for the model-data mismatch in the ENSO-AC relationship is that uncertainties in AC amplitude estimates from corals are more uncertain than depicted by the bootstrap intervals, as documented by discrepancies of up to 30% in AC estimates from overlapping coral δ^{18}O records from the central tropical Pacific (Supplementary Figure S12). The relationship

between $\delta^{18}O$ and SSS is poorly constrained on subannual scales, and may vary across a given reef environment, further confounding estimates of AC amplitude changes from high-resolution archives. Results are, however, insensitive to the choice of ENSO metric as long as fossil/modern ratios are used (Supplementary Figure S27).

Changes in the spatial characteristics of ENSO represent another source of uncertainty, as different flavors of ENSO have different impacts on SST and SSS across the study domain. Canonical El Niño events involve temperature changes in the eastern Pacific (EP). However, many events peak in the CP[43]. Indeed, changes in the prevalence of ENSO flavors in the Holocene have been suggested by changes in the asymmetry of ENSO anomalies in the eastern Pacific[26] as well as analysis of PMIP3 *midHolocene* simulations[12,44]. Thus, some of the observed variations in ENSO intensity/frequency over the Holocene could reflect changes in the spatial pattern of ENSO and differences between individual records could reflect a dominance of one expression of ENSO over another[26]. However, an empirical ENSO model suggests that modern changes in the prevalence of ENSO flavors may arise internally[45]. Our dataset is too sparse to resolve spatial features of ENSO or the AC structure, but it is hoped that denser proxy networks will shed light on these questions in the future.

Implications for ENSO dynamics

It has been suggested that boreal fall insolation, which peaks at $\sim$5 kyBP (Supplementary Figure S8), modulates ENSO variability via air/sea coupling strength[8]. Our analyses reveal that changes in

ENSO variance and AC amplitude over the Holocene bear no simple relation to orbital forcing, excluding a linear mechanism. It is possible that millennial-scale changes in ENSO variability arose either (1) internally, (2) as a non-linear response to orbital forcing, or (3) because of other factors, such as the presence of a remnant Laurentide ice sheet, which modulated the response to orbital forcing[46]. Our observations suggest persistent changes in ENSO variance and AC amplitude that fall well outside the range shown by both *piControl* and *midHolocene* PMIP3 simulations, particularly during the 3-5 kyBP interval. The PMIP3 ensemble does not capture the potential range of ENSO variability over this interval, which should become a key target for climate models of varying complexity to simulate and explain. One challenge in simulating such changes with GCMs is that computational requirements restrict simulations to 200-500yrs, on average. Additional long transient runs, both forced[13] and unforced[41], would help distinguish endogenous from exogenous sources of ENSO variability. Furthermore, the simulated relationship between ENSO variance and AC amplitude is incompatible with observations. GCMs where an inverse relationship to AC amplitude dominates the ENSO response to orbital forcing may therefore not be representative of the real world. Given that the mean state, AC and ENSO are so tightly connected[16,47], the substantial climatological biases in CMIP5 models[48] are a logical suspect for this exaggerated relationship. Of particular relevance is the SST-shortwave feedback[49], the asymmetric nature of which is not captured by many state-of-the-art GCMs[48]. Even those GCMs that qualitatively simulate the feedback may do so via error compensation, so we speculate that large improvements in ENSO simulations would result from a correct representation of the underlying processes.

While precessional and greenhouse gas forcing are fundamentally different in character, our

work demonstrates the ability of high-resolution palaeoclimate records to provide fundamental constraints on tropical climate dynamics, as represented in models used to project twenty-first century climate trends. In that context, the fact that ENSO seemed relatively impervious to a large external forcing suggests that processes internal to the climate system could dominate external influences. Understanding internal processes of low-frequency ENSO modulation, and the extent to which they are captured by climate models, is therefore of utmost importance to improving climate projections.

Extended Methods

Observational synthesis. We compiled isotopic records obtained on coral or mollusks from 65 sites in the Pacific (Table S1). The majority of the records have been published[5, 6, 24–26, 28–37], but some are published for the first time here (Supplementary Information). Most of the individual records are comparatively short (50 years or less, Supplementary Figure 1). The records sample 2162 years out of the past 10,000 years (Supplementary Figure 1, Supplementary Table 1).

For analytical purposes, we group the individual sites into three separate regions:

West [120, 180, 20°S, 0°N], including Papua New Guinea and New Caledonia

Center [170°W, 120°W, 5°S, 5°N], corresponding to the NINO3.4 region (for which the SST average is a key ENSO indicator) and encompassing part of the Line Islands.

East [90°W, 80°W, 5°S, 5°N], corresponding to the NINO1+2 regions, a primary region to moni-

tor coastal warming.

Figure 1 shows that these three climatically-meaningful regions encompass the majority of the sites. Note that the sites of ref 26, while formally outside the NINO1+2 region (eastern box) are interpreted as reflecting NINO1+2 SST[35].

Analysis of observations. Changes in ENSO variance were quantified by computing the ratio of fossil to modern variance in the 2-7y band. In continuous records, the latter was isolated via a (Morlet) wavelet filter (Supplementary Figure 7), while for peruvian mollusks we used the ratio of fossil to modern variance of the distribution of the annual cycle amplitude[35], a proxy for NINO1+2 interannual variance. Results are not sensitive to the filter type or exact metric (Supplementary Information). AC amplitude was quantified as the range (maximum minus minimum) of a monthly-mean seasonal cycle evaluated over each record's time span after high-pass filtering the data with a 10-year smoothing spline[50,51] to avoid the biasing effect of trends. Changes in this quantity were, likewise, computed as a ratio between fossil and modern samples.

Uncertainties in both quantities were estimated via a block-bootstrap procedure[52,53] with 1,000 draws. For interannual variance, the block length was set at 2 years, while for seasonal amplitude the block length was set to the number of samples per year. Both choices reflect a compromise between the approximate decorrelation time of the records and the shortness of some proxy records. For peruvian mollusks, uncertainties were estimated via Monte Carlo simulations as described in ref 54. The procedure is similar to a block-bootstrap analysis with 5000 draws

and block lengths of 1 year using an instrumental time series sampled and disturbed by simulated proxy-related noises.

Forward modeling of marine bicarbonates. Although $\delta^{18}\mathrm{O}$ in marine biocarbonates predominantly reflects either SST[55–57] or seawater $\delta^{18}\mathrm{O}$ variations resulting from net surface freshwater balance[58,59], most corals and mollusks are affected by both variables. This problem may be directly addressed by explicitly modeling the relationship between the environmental variables and the observed $\delta^{18}\mathrm{O}$ (i.e. forward modeling[40,60]). Unlike empirical calibration, forward models do not require assumptions to be made about linearity, the independence of predictors, or the normality of residuals.

A reasonably complete model of the incorporation of $^{18}\mathrm{O}$ in coral aragonite requires information on local ocean temperature, seawater $^{18}\mathrm{O}$, pH, insolation and nutrients. However, ref 39 developed a simple bivariate model to predict the $^{18}\mathrm{O}$ of coral aragonite using SST and SSS as sole inputs. SSS acts as a proxy for seawater $^{18}\mathrm{O}$, with a regionally-dependent coefficients calibrated over the instrumental era. The thermal dependence is set at $-0.22‰/°\mathrm{C}$, close to the expected slope for inorganic equilibrium fractionation[61]. This model has been shown to capture first-order variations in the hydrological response of coral $^{18}\mathrm{O}$[39,62]. There are known limitations to the use of such a simple model[62–64]. Specifically, it ignores coral biology and non-equilibrium effects, which are thought to explain some low-frequency trends in corals[65]. Further, the SSS-$^{18}\mathrm{O}_{\mathrm{sw}}$ slope may not be constant on millennial timescales[66], and its spatial variations may severely bias the estimation of paleo-ENSO variability, particularly in the western Pacific[62]. Nevertheless, we use this model

to translate climate model outputs into a $^{18}\mathrm{O}$ signal for comparison with the observations because very few of the climate models explicitly simulate water isotopes. The same model may be applied to simulate $\delta^{18}\mathrm{O}$ values in the shells of *Tridacna sp* and *Mesodesma donacium*[26,36,37] since they precipitate aragonite like corals. The slope of the SST-$\delta^{18}\mathrm{O}$ relationship generally used for aragonitic mollusks ranges from -0.21 to $-0.27‰/°\mathrm{C}$[67,68], compatible with the slope of $-0.22‰/°\mathrm{C}$ used by ref 39.

We note that recent studies have attempted to quantify uncertainties in inferring changes in ENSO variance from calibrated proxy observations[42,69]. By using a process model, we eschew some of the difficulties associated with calibration, but this passes the uncertainties on to the process model. Additionally, ref 69 neglected sampling uncertainties, which are central to our analysis. The existence of non-climatic noise is a problem in every paleoclimate dataset, and the reader is referred to the original studies for an appraisal of the strength of each climate signal.

Climate Models and Simulations. We consider the simulations that have been run as part of the fifth phase of the Coupled Modeling Intercomparison Project (CMIP5)[70] and analyzed in the third phase of the Palaeoclimate Modelling Intercomparison Project (PMIP3)[27]. This set of simulations is usually referred to as the CMIP5/PMIP3 experiments, although here we simply refer to them as PMIP3 experiments. The models used (Supplementary Table 2) are state-of-the-art coupled ocean atmosphere general circulation models (GCMs), or Earth system models (ESMs) with different levels of complexity in the forcing used or in the interactions between climate and the carbon cycle[71]. We consider three experimental designs, following PMIP3 nomenclature:

piControl

The reference are pre-industrial simulations for which Earth's orbit and solar constant are representative of modern conditions, and trace gases, land use and aerosols are prescribed to AD 1850. The prescribed values vary slightly from one model to the other. Details are given in `https://wiki.lsce.ipsl.fr/pmip3/doku.php/pmip3:design:pi:final`.

midHolocene

For the mid-Holocene we use simulations in which Earth orbital parameters and trace gases have been prescribed to those valid for 6ka[27]. In all the simulations the date of the vernal equinox is fixed to March 21 at noon. The insolation forcing at the equator is displayed in Supplementary Figure 9 (see also ref 72, Fig. 3). Details are given in `https://wiki.lsce.ipsl.fr/pmip3/doku.php/pmip3:design:6k:final`.

Historical

To test the impact of the reference period on the analyses of the simulated change in the different climates we also consider historical simulations[70] forced with time evolution of trace gases, volcanic forcing and land-use over the period 1860-2005. We sampled from the full ensemble of HIST simulations, including several runs with slightly different initial conditions for each model. In general, their ENSO statistics were indistinguishable from PI within uncertainties.

Analysis of GCM simulations. GCM-simulated SST and SSS were translated to $\delta^{18}O$ values via a forward model[39]. Pseudocoral averages over the three main regions (WP, CP, EP) were then resampled using the above-mentioned block-bootstrap procedure with $N = 1,000$ draws, before being subsampled on contiguous 50-year blocks to emulate short observational windows (Supplementary Information, Supplementary Figures S13-S22). We then computed ENSO variance and AC amplitude, as well as their ratios, for each ensemble member. Probability distributions from these 1,000 member ensembles were then obtained via kernel density estimation with a bandwidth $h = 0.15$ (Figure 2).

Regression Analysis. We use total least squares (TLS) regression (a form of error-in-variables modeling, closely connected to orthogonal regression[73]), to account for uncertainties in the ENSO - AC amplitude relationship. TLS steepens regression slopes by taking the potentially biasing effects of observational noise into account[74]. ENSO variance and AC amplitude ratios were scaled by their uncertainty (measured by the interquartile range of their block-bootstrap distributions) prior to TLS regression, to ensure homogenous error magnitudes on both axes of Figure 3. Uncertainties in regression parameters are estimated via a bootstrap approach[75], with 2,000 draws.

Wavelet Analysis. The relationship between ENSO and the AC is also probed via Morlet wavelet analysis[76]. We sum the energies corresponding to the 2-7y and 0.8-1.2 y bands and report linear correlations between the resulting series[19]. We do so for all seasonally-resolved, continuous records in the database (i.e. all except those of refs 26 and 6) and for the PMIP3 *piControl* and *midHolocene* model outputs, separately for each of the three geographic regions. Statistical signif-

icance is established via a non-parametric, isospectral test[77], which accounts for the loss of degrees of freedom imparted by smoothing by low-frequency wavelets.

Data. Data for the paleo observations and model output for the 3 boxes outlined in Fig. 1, is available via (https://github.com/CommonClimate/EmileGeay_NatGeo2015). The original model data was obtained via the CMIP5/PMIP3 (http://cmip-pcmdi.llnl.gov/cmip5/) web site, while the published paleo data were obtained from the National Climatic Data Center (https://www.ncdc.noaa.gov/data-access/paleoclimatology-data).

Code Availability. Matlab/Python code to reproduce the block bootstrap, wavelet and regression analysis is available at https://github.com/CommonClimate/EmileGeay_NatGeo2015. In particular, these codes generate the probability distributions for all the ratios plotted in Fig. 2, except those associated with ref 26. The Matlab code to generate the latter distributions is available at http://www.isem.univ-montp2.fr/carre_matthieu, using the parameter values published in ref 54 (SOM).

Bibliography

1. Sarachik, E. S. & Cane, M. A. *The El Niño-Southern Oscillation Phenomenon*. 336 pages (Cambridge University Press, Cambridge, UK, 2010).

2. Collins, M. *et al.* The impact of global warming on the tropical Pacific Ocean and El Niño. *Nature Geosci* **3**, 391–397 (2010).

3. Schmidt, G. A. Enhancing the relevance of palaeoclimate model/data comparisons for assessments of future climate change. *Journal of Quaternary Science* **25**, 79–87 (2010).

4. Braconnot, P., Luan, Y., Brewer, S. & Zheng, W. Impact of Earth's orbit and freshwater fluxes on Holocene climate mean seasonal cycle and ENSO characteristics. *Climate Dynamics* **38**, 1081–1092 (2012).

5. Tudhope, A. W. *et al.* Variability in the El Niño-Southern Oscillation through a glacial-interglacial cycle. *Science* **291**, 1511–1517 (2001).

6. McGregor, H. V. & Gagan, M. K. Western Pacific coral δ^{18}O records of anomalous Holocene variability in the El Niño-Southern Oscillation. *Geophysical Research Letters* **31** (2004).

7. Koutavas, A. & Joanides, S. El Niño-Southern Oscillation extrema in the Holocene and Last Glacial Maximum. *Paleoceanography* **27**, PA4208 (2012).

8. Clement, A. C., Seager, R. & Cane, M. A. Suppression of El Niño during the mid-Holocene by changes in the Earth's orbit. *Paleoceanography* **15**, 731–737 (2000).

9. Liu, Z., Kutzbach, J. & Wu, L. Modeling climate shift of El Niñovariability in the Holocene. *Geophysical Research Letters* **27**, 2265–2268 (2000).

10. Zheng, W., Braconnot, P., Guilyardi, E., Merkel, U. & Yu, Y. ENSO at 6ka and 21ka from ocean–atmosphere coupled model simulations. *Clim. Dyn.* **30**, 745–762 (2008).

11. Chiang, J. C. H., Fang, Y. & Chang, P. Pacific Climate Change and ENSO Activity in the Mid-Holocene. *Journal of Climate* **22**, 923–939 (2009).

12. An, S.-I. & Choi, J. Mid-Holocene tropical Pacific climate state, annual cycle, and ENSO in PMIP2 and PMIP3. *Climate Dynamics* **43**, 957–970 (2014).

13. Liu, Z. *et al.* Evolution and forcing mechanisms of El Niño over the past 21,000 years. *Nature* **515**, 550–553 (2014).

14. Wang, X. L. The coupling of the annual cycle and ENSO over the tropical Pacific. *Journal of the Atmospheric Sciences* **51**, 1115–1136 (1994).

15. Chang, P., Wang, B., Li, T. & Ji, L. Interactions between the seasonal cycle and the Southern Oscillation - Frequency entrainment and chaos in a coupled ocean-atmosphere model. *Geophys. Res. Lett.* **21**, 2817–2820 (1994).

16. Guilyardi, E. El Niño mean state seasonal cycle interactions in a multi-model ensemble. *Clim. Dyn.* **26**, 329–348 (2006).

17. Timmermann, A., Lorenz, S. J., An, S.-I., Clement, A. & Xie, S.-P. The effect of orbital forcing on the mean climate and variability of the tropical pacific. *Journal of Climate* **20**, 4147–4159 (2007).

18. An, S.-I. *et al.* The inverse effect of annual-mean state and annual-cycle changes on ENSO. *Journal of Climate* **23**, 1095–1110 (2010).

19. An, S.-I. & Choi, J. Inverse relationship between the equatorial eastern Pacific annual-cycle and ENSO amplitudes in a coupled general circulation model. *Climate Dynamics* **40**, 663–675 (2013).

20. Liu, Z. A simple model study of ENSO suppression by external periodic forcing. *J. Clim.* **15**, 1088–1098 (2002).

21. Tziperman, E., Stone, L., Cane, M. A. & Jarosh, H. El Niño chaos: overlapping of resonances between the seasonal cycle and the Pacific ocean-atmosphere oscillator. *Science* **264**, 72–74 (1994).

22. Jin, F.-F., Neelin, J. D. & Ghil, M. El Niño on the Devil's staircase: annual subharmonic steps to chaos. *Science* **264**, 70–72 (1994).

23. Stuecker, M. F., Timmermann, A., Jin, F.-F., McGregor, S. & Ren, H.-L. A combination mode of the annual cycle and the El Niño-Southern Oscillation. *Nature Geosci* **6**, 540–544 (2013).

24. McGregor, H. V. *et al.* A weak El Niño-Southern Oscillation with delayed seasonal growth around 4,300 years ago. *Nature Geoscience* **6**, 949–953 (2013).

428 25. Cobb, K. M. *et al.* Highly variable El Niño-Southern Oscillationthroughout the Holocene.
429 *Science* **339**, 67–70 (2013).

430 26. Carré, M. *et al.* Holocene history of ENSO variance and asymmetry in the eastern tropical
431 Pacific. *Science* **345**, 1045–1048 (2014).

432 27. Braconnot, P. *et al.* Evaluation of climate models using palaeoclimatic data. *Nature Clim.*
433 *Change* **2**, 417–424 (2012).

434 28. Cobb, K. M., Charles, C. D., Cheng, H. & Edwards, R. L. El Niño/Southern Oscillation and
435 tropical Pacific climate during the last millennium. *Nature* **424**, 271–276 (2003).

436 29. Duprey, N. *et al.* Early mid-Holocene SST variability and surface-ocean water balance in the
437 southwest Pacific. *Paleoceanography* **27**, PA4207 (2012).

438 30. Kilbourne, K. H., Quinn, T. M., Taylor, F. W., Delcroix, T. & Gouriou, Y. El Niño-Southern
439 Oscillation-related salinity variations recorded in the skeletal geochemistry of a *Porites* coral
440 from Espiritu Santo, Vanuatu. *Paleoceanography* **19**, PA4002 (2004).

441 31. Woodroffe, C. D. & Gagan, M. K. Coral microatolls from the central Pacific record Late
442 Holocene El Niño. *Geophysical Research Letters* **27**, 1511–1514 (2000).

443 32. Woodroffe, C. D., Beech, M. R. & Gagan, M. K. Mid-late Holocene El Niño variability in the
444 equatorial Pacific from coral microatolls. *Geophysical Research Letters* **30**, 1358 (2003).

445 33. Evans, M., Fairbanks, R. & Rubenstone, J. A proxy index of ENSO teleconnections. *Nature*
446 **394**, 732–733 (1998).

34. McGregor, H. V., Fischer, M. J., Gagan, M. K., Fink, D. & Woodroffe, C. D. Environmental control of the oxygen isotope composition of *Porites* coral microatolls. *Geochimica et Cosmochimica Acta* **75**, 3930–3944 (2011).

35. Carré, M., Sachs, J. P., Schauer, A. J., Rodríguez, W. E. & Ramos, F. C. Reconstructing El Niño-Southern Oscillation activity and ocean temperature seasonality from short-lived marine mollusk shells from Peru. *Palaeogeography, Palaeoclimatology, Palaeoecology* **371**, 45–53 (2013).

36. Driscoll, R. *et al.* ENSO Reconstructions over the past 60 ka using giant clams (*Tridacna sp.*) from Papua New Guinea. *Geophysical Research Letters* **41**, 6819–6825 (2014).

37. Welsh, K., Elliot, M., Tudhope, A., Ayling, B. & Chappell, J. Giant bivalves (*Tridacna gigas*) as recorders of ENSO variability. *Earth and Planetary Science Letters* **307**, 266–270 (2011).

38. McGregor, S., Timmermann, A., England, M. H., Elison Timm, O. & Wittenberg, A. T. Inferred changes in El Niño-Southern Oscillation variance over the past six centuries. *Climate of the Past* **9**, 2269–2284 (2013).

39. Thompson, D. M., Ault, T. R., Evans, M. N., Cole, J. E. & Emile-Geay, J. Comparison of observed and simulated tropical climate trends using a forward model of coral δ^{18}O. *Geophys. Res. Lett.* **38**, L14706 (2011).

40. Dee, S. G. *et al.* PRYSM: an open-source framework for proxy system modeling, with applications to oxygen-isotope systems. *J. Adv. Mod. Earth Sys.* **07** (2015).

41. Wittenberg, A. T. Are historical records sufficient to constrain ENSO simulations? *Geophys. Res. Lett.* **36**, L12702 (2009).

42. Russon, T., Tudhope, A. W., Hegerl, G. C., Schurer, A. & Collins, M. Assessing the significance of changes in ENSO amplitude using variance metrics. *Journal of Climate* **27**, 4911–4922 (2014).

43. Kug, J.-S., Jin, F.-F. & An, S.-I. Two types of El Niño events: Cold tongue El Niño and warm pool El Niño. *Journal of Climate* **22**, 1499–1515 (2009).

44. Karamperidou, C., Di Nezio, P. N., Timmermann, A., Jin, F.-F. & Cobb, K. M. The response of ENSO flavors to mid-Holocene climate: Implications for proxy interpretation. *Paleoceanography* **30**, 527–547 (2015).

45. Newman, M., Shin, S.-I. & Alexander, M. A. Natural variation in ENSO flavors. *Geophys. Res. Lett.* **38** (2011).

46. Luan, Y., Braconnot, P., Yu, Y. & Zheng, W. Tropical Pacific mean state and ENSO changes: sensitivity to freshwater flux and remnant ice sheets at 9.5 ka BP. *Climate Dynamics* **44**, 661–678 (2015).

47. Roberts, W. H. G., Battisti, D. S. & Tudhope, A. W. ENSO in the mid-Holocene according to CSM and HadCM3. *Journal of Climate* **27**, 1223–1242 (2013).

48. Bellenger, H., Guilyardi, E., Leloup, J., Lengaigne, M. & Vialard, J. ENSO representation in climate models: from CMIP3 to CMIP5. *Climate Dynamics* **42**, 1999–2018 (2014).

485 49. Lloyd, J., Guilyardi, E. & Weller, H. The Role of Atmosphere Feedbacks during ENSO in the
486 CMIP3 Models. Part III: The Shortwave Flux Feedback. *Journal of Climate* **25**, 4275–4293
487 (2012).

488 50. Cook, E. R. & Peters, K. The smoothing spline: A new approach to standardizing forest
489 interior tree-ring width series for dendroclimatic studies. *Tree-Ring Bulletin* **41**, 45–53 (1981).

490 51. Weinert, H. L. A fast compact algorithm for cubic spline smoothing. *Computational Statistics*
491 *& Data Analysis* **53**, 932–940 (2009).

492 52. Efron, B. & Tibshirani, R. J. *An Introduction to the Bootstrap* (Chapman & Hall, New York,
493 1993).

494 53. Kunsch, H. R. The jackknife and the bootstrap for general stationary observations. *The Annals*
495 *of Statistics* **17**, 1217–1241 (1989).

496 54. Carré, M., Sachs, J. P., Wallace, J. M. & Favier, C. Exploring errors in paleoclimate proxy
497 reconstructions using monte carlo simulations: paleotemperature from mollusk and coral geo-
498 chemistry. *Climate of the Past* **8**, 433–450 (2012).

499 55. Dunbar, R. B., Wellington, G. M., Colgan, M. W. & Glynn, P. W. Eastern Pacific sea sur-
500 face temperature since 1600 A.D.: The δ^{18}Orecord or climate variability in Galápagos corals.
501 *Paleoceanography* **9**, 291–316 (1994).

502 56. Evans, M., Fairbanks, R. & Rubenstone, J. The thermal oceanographic signal of
503 El Niñoreconstructed from a Kiritimati Island coral. *Journal of Geophysical Research*
504 *(Oceans)* **104**, 13409–13422 (1999).

505 57. Cobb, K. M., Charles, C. D. & Hunter, D. E. A central tropical Pacific coral demonstrates
506 Pacific, Indian, and Atlantic decadal climate connections. *Geophys. Res. Lett.* **28**, 2209–2212
507 (2001).

508 58. Fairbanks, R. G. *et al.* Evaluating climate indices and their geochemical proxies measured in
509 corals. *Coral Reefs* **16**, S93–S100 (1997).

510 59. Conroy, J. L., Cobb, K. M., Lynch-Stieglitz, J. & Polissar, P. J. Constraints on the salinity–
511 oxygen isotope relationship in the central tropical pacific ocean. *Marine Chemistry* **161**, 26–33
512 (2014).

513 60. Evans, M. N., Tolwinski-Ward, S. E., Thompson, D. M. & Anchukaitis, K. J. Applications of
514 proxy system modeling in high resolution paleoclimatology. *Quaternary Science Reviews* **76**,
515 16–28 (2013).

516 61. McConnaughey, T. ^{13}C and ^{18}O isotopic disequilibrium in biological carbonates: I. Patterns.
517 *Geochim. Cosmochim. Act.* **53**, 151–162 (1989).

518 62. Russon, T., Tudhope, A. W., Hegerl, G. C., Collins, M. & Tindall, J. Inter-annual tropical
519 Pacific climate variability in an isotope-enabled CGCM: implications for interpreting coral
520 stable oxygen isotope records of ENSO. *Climate of the Past* **9**, 1543–1557 (2013).

521 63. Stevenson, S., McGregor, H. V., Phipps, S. J. & Fox-Kemper, B. Quantifying errors in coral-
522 based ENSO estimates: Toward improved forward modeling of δ^{18}O. *Paleoceanography* **28**,
523 633–649 (2013).

524 64. Thompson, D. M. *et al.* Coral-model comparison highlighting the role of salinity in long-term
525 trends. *PAGES Newsletter* **21**, 60–61 (2013).

526 65. Lough, J. A strategy to improve the contribution of coral data to high-resolution paleoclima-
527 tology. *Palaeogeography, Palaeoclimatology, Palaeoecology* **204**, 115 – 143 (2004).

528 66. LeGrande, A. N. & Schmidt, G. A. Water isotopologues as a quantitative paleosalinity proxy.
529 *Paleoceanography* **26**, PA3225 (2011).

530 67. Grossman, E. L. & Ku, T.-L. Oxygen and carbon isotope fractionation in biogenic aragonite:
531 Temperature effects. *Chemical Geology: Isotope Geoscience section* **59**, 59–74 (1986).

532 68. Carré, M. *et al.* Stable isotopes and sclerochronology of the bivalve *Mesodesma donacium*: Po-
533 tential application to Peruvian paleoceanographic reconstructions. *Palaeogeography, Palaeo-*
534 *climatology, Palaeoecology* **228**, 4–25 (2005).

535 69. Russon, T., Tudhope, A. W., Collins, M. & Hegerl, G. C. Inferring changes in ENSO amplitude
536 from the variance of proxy records. *Geophysical Research Letters* 2014GL062331 (2015).

537 70. Taylor, K. E., Stouffer, R. J. & Meehl, G. A. An overview of CMIP5 and the experiment
538 design. *Bulletin of the American Meteorological Society* **93**, 485–498 (2011).

539 71. Flato, G. *et al.* Evaluation of Climate Models. In Stocker, T. F. *et al.* (eds.) *Climate Change*
540 *2013: The Physical Science Basis. Contribution of Working Group I to the Fifth Assessment*
541 *Report of the Intergovernmental Panel on Climate Change*, 741–866 (Cambridge University
542 Press, Cambridge, United Kingdom and New York, NY, USA, 2013).

543 72. Luan, Y., Braconnot, P., Yu, Y., Zheng, W. & Marti, O. Early and mid-Holocene climate in
544 the tropical Pacific: seasonal cycle and interannual variability induced by insolation changes.
545 *Climate of the Past* **8**, 1093–1108 (2012).

546 73. Van Huffel, S. *Total least squares and errors-in-variables modeling: bridging the gap between*
547 *statistics, computational mathematics and engineering*, 539–555 (Physica-Verlag HD, 2004).

548 74. Markovsky, I., Sima, D. M. & Van Huffel, S. Total least squares methods. *Wiley Interdisci-*
549 *plinary Reviews: Computational Statistics* **2**, 212–217 (2010).

550 75. Pešta, M. Total least squares and bootstrapping with applications in calibration. *Statistics* **47**,
551 966–991 (2013).

552 76. Torrence, C. & Compo, G. P. A practical guide to wavelet analysis. *Bull. Amer. Meteor. Soc.*
553 **79**, 61–78 (1998).

554 77. Ebisuzaki, W. A method to estimate the statistical significance of a correlation when the data
555 are serially correlated. *Journal of Climate* **10**, 2147–2153 (1997).

556 **Supplementary Information** is linked to the online version of the paper at `www.nature.`
557 `com/ngeo`.

558 **Acknowledgements**

559 We thank the referees for constructive reviews that improved the manuscript. All data, metadata
560 and code [will be] archived at `zenodo.org`. We acknowledge the World Climate Research Pro-

gram's Working Group on Coupled Modelling, which is responsible for CMIP, and we thank the PMIP3 modeling groups for producing and making available their model output. The U.S. Department of Energy's Program for Climate Model Diagnosis and Intercomparison provides coordinating support for CMIP, and led development of software infrastructure in partnership with the Global Organization for Earth System Science Portals. JEG acknowledges support from US NSF grant DMS 1025465. KMC acknowledges support from NOAA award NA11OAR4310166 and NSF award OCE-0752091. M. Collins acknowledges support from UK NERC grant NE/H009957/1. HVM and AT acknowledge support from Australian Research Council (ARC) Discovery Project grant DP1092945. HVM is supported by an ARC Future Fellowship FT140100286 grant. AT acknowledges support from UK NERC grant NE/H009957/1. TC thanks M. McCulloch (formerly at ANU) for dating the Bayes coral, and M. Gagan's team at ANU for help with isotopic measurements. The Bayes 1 core was collected with funds from the Institut de Recherche pour le Développement. BS was supported by the DFG Cluster of Excellence "The Future Ocean" (EXC 80/2). PB, M. Carré, TC, JL, ME and AT were supported by the French National Research Agency under EL PASO grant (no. 2010 298 BLANC 608 01). This project also serves for coordination and implementation of the PMIP3/CMIP5 simulations on the ESGF distributed database. We thank Jean-Yves Peterschmitt for his help with the PMIP database. This work was initiated in a workshop co-sponsored by WCRP/CLIVAR, IGBP/PAGES, INQUA, and IPSL in 2011.

Author Contributions

J.E.G. designed the study, performed the analysis, lead the writing, and prepared the manuscript. P.B. coordinated the synthesis. M.Carré, K.M.C, T.C., M.E. and R.D. contributed data and/or analysis. P.B. and J.L. analyzed simulations and contributed to writing. Y.Z. processed PMIP3 output and generated some of the supplementary figures. A.T., B.S., M.Collins provided input in the analysis and interpretation. J.E.G., K.M.C., M.Carré, S.P.H., H.V.M., T.C., P.B. and A.T. wrote the paper. All authors reviewed the manuscript.

Author information

Reprints and permissions information is available at `www.nature.com/reprints`. The authors declare no competing financial interests. Correspondence and requests for materials should be addressed to julieneg@usc.edu.

Figure 1 Location and ENSO sensitivity of proxy archives. Circles denote corals, stars denote mollusks. Contours denote biocarbonate $\delta^{18}\mathrm{O}$ composites (‰ per °C of NINO3.4 SST) derived from the model of Thompson et al.[39] driven by NCEP OI analysis v2 SST and SODA 2.2.4 SSS over 1981-2010 boreal winters (Supplementary Figures S8-S9). $\delta^{18}\mathrm{O}$ values were regressed onto NINO3.4 SST to highlight relationships to ENSO. The three equatorial study regions (West, Center & East) are delineated by boxes. Note that refs. 11,12,15,16,18-21 all use data from Kiritimati ($1°53'$N,$157°24'W$).

Figure 2 (top) Changes in ENSO variance and AC amplitude over the Holocene. LEFT column: Changes in ENSO-band (2-7y) variance between fossil and modern samples in the West (top), Center (middle) and East (bottom). Horizontals bars mark the period covered by each dataset; except for mollusks from the Peruvian coast, these are narrower than the symbol width. Ellipses represent uncertainties about these ratios in both dimensions: the width represents a 95% CI for the central date of each sample, based on reported analytical uncertainty on radiometric ages; the vertical component is a 95% CI for the variance ratio, obtained via a block-bootstrap procedure (Methods). Unity (no change) is marked by a dashed gray line. Similar statistics derived from PMIP3 models on 50-year windows are depicted on side panels for *piControl* and *midHolocene* experiments. Solid lines are kernel density estimates of those distributions (Methods), while dashed lines indicate their median. RIGHT column: idem for AC amplitude.

[h]

		Quantiles		
Period	**Region**	2.5%	50%	97.5%
5.5 – 7.5 kyBP	West	-125%	50%	92%
	Center	-5%	66%	92%
	East	-16%	33%	69%
3–5 kyBP	West	-54%	35%	61%
	Center	28%	64%	84%
	East	-18%	58%	109%

Table 1: Observed reductions in ENSO variance in the tropical Pacific during the MH (5.5–7.5 kyBP) and the 3-5 kyBP interval. The numbers represent quantiles of the block-bootstrap ensembles. By convention, a negative reduction implies an increase.

[h]

H_0	HadGEM2	GISS	KCM	CCSM4	MIROC	MPI	CNRM	IPSL	CSIRO
PI null	1.37%	11.98%	1.62%	3.66%	2.82%	3.55%	0.88%	2.06%	5.00%
MH null	3.12%	3.16%	3.35%	5.60%	7.36%	9.78%	3.81%	15.50%	0.21%

Table 2: Probability of observing periods of reduced ENSO activity in the CP in nine GCMs. Top row: frequency of occurrence of 50-year long periods for which the ENSO variance ratio is as low as the 3-5 kyBP average inferred from paleoclimate observations (0.36 – a 64% reduction) in pre-industrial (*piControl*) simulations. Bottom row: same for *midHolocene* simulations

Figure 3 (top) Link between ENSO variance and the seasonal cycle in proxy observations (top) and PMIP3 models (bottom). The observed values are for all seasonally-resolved records from the Pacific during the whole of the past 10 ky. The simulated values are based on 50-year segments from the *midHolocene* and *piControl* simulations. On top, symbology as in Figure 1. On the bottom, triangles denote the median of *piControl* simulations, squares the median of *midHolocene* simulations. Data from the eastern, central and western Pacific were pooled together, scaled by their interquartile range so their uncertainties on both axes are commensurate. An orthogonal regression (total least squares) fit is presented for both datasets, together with approximate 95% CIs (dashed lines) and probability density (gray contours) obtained via bootstrap resampling (Methods).

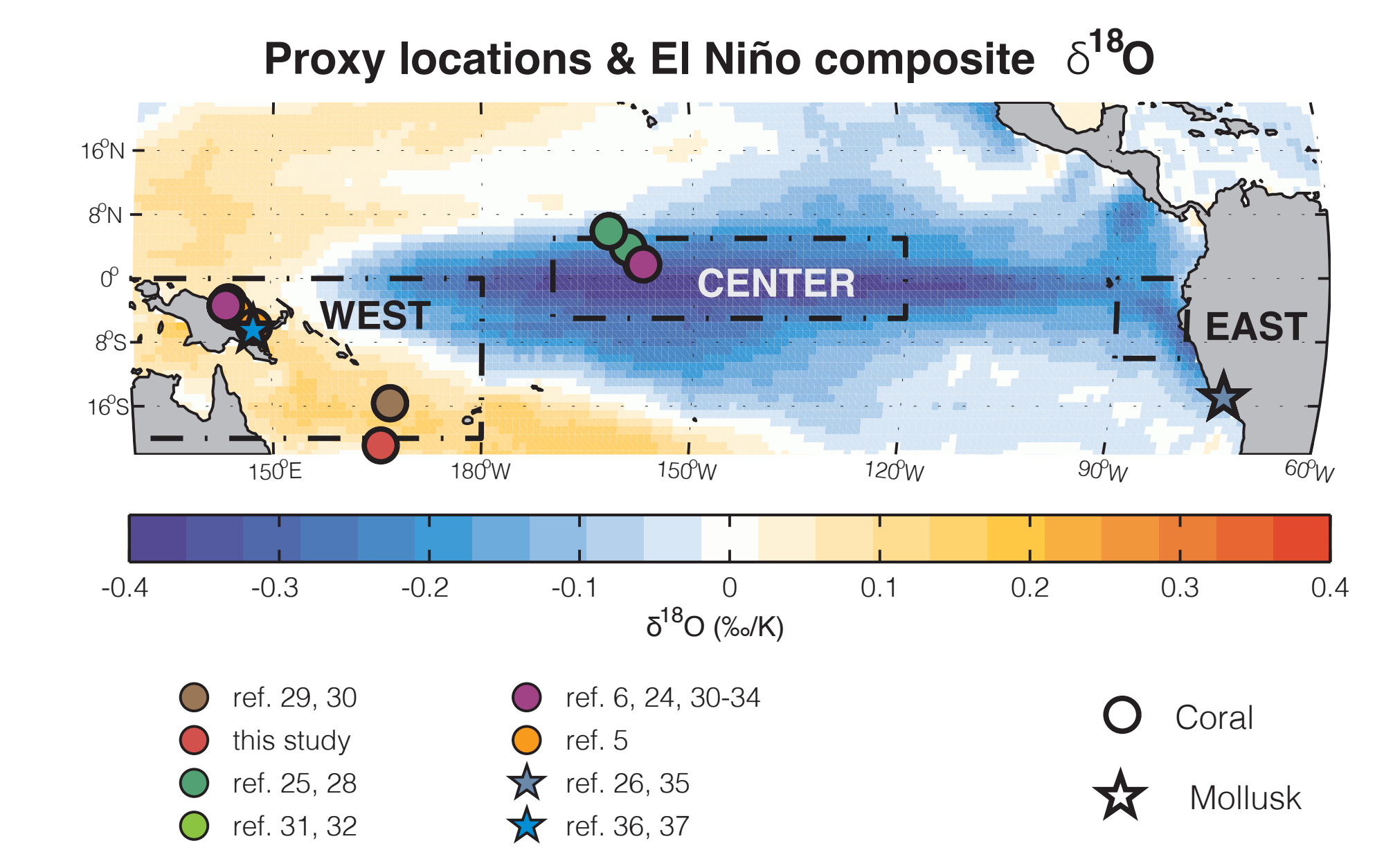
Proxy locations & El Niño composite δ18O
16°N
8°N
0°
8°S
16°S
150°E
180°W
150°W
120°W
90°W
60°W
WEST
CENTER
EAST
-0.4
-0.3
-0.2
-0.1
0
0.1
0.2
0.3
0.4
δ18O (‰/K)
ref. 29, 30
this study
ref. 25, 28
ref. 31, 32
ref. 6, 24, 30-34
ref. 5
ref. 26, 35
ref. 36, 37
Coral
Mollusk

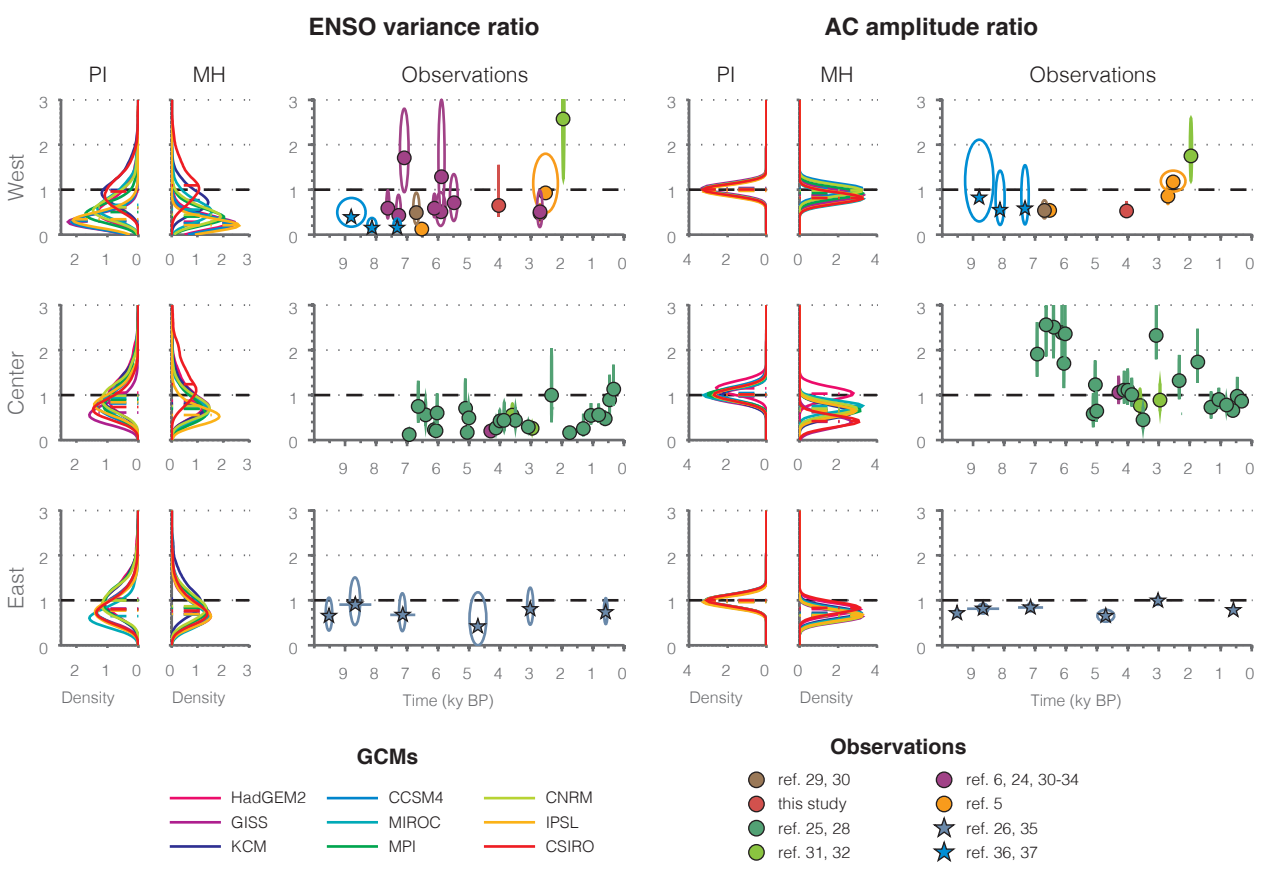
ENSO variance ratio
AC amplitude ratio
PI
MH
Observations
West
Center
East
Density
Time (ky BP)
GCMs
HadGEM2
GISS
KCM
CCSM4
MIROC
MPI
CNRM
IPSL
CSIRO
Observations
ref. 29, 30
this study
ref. 25, 28
ref. 31, 32
ref. 6, 24, 30-34
ref. 5
ref. 26, 35
ref. 36, 37

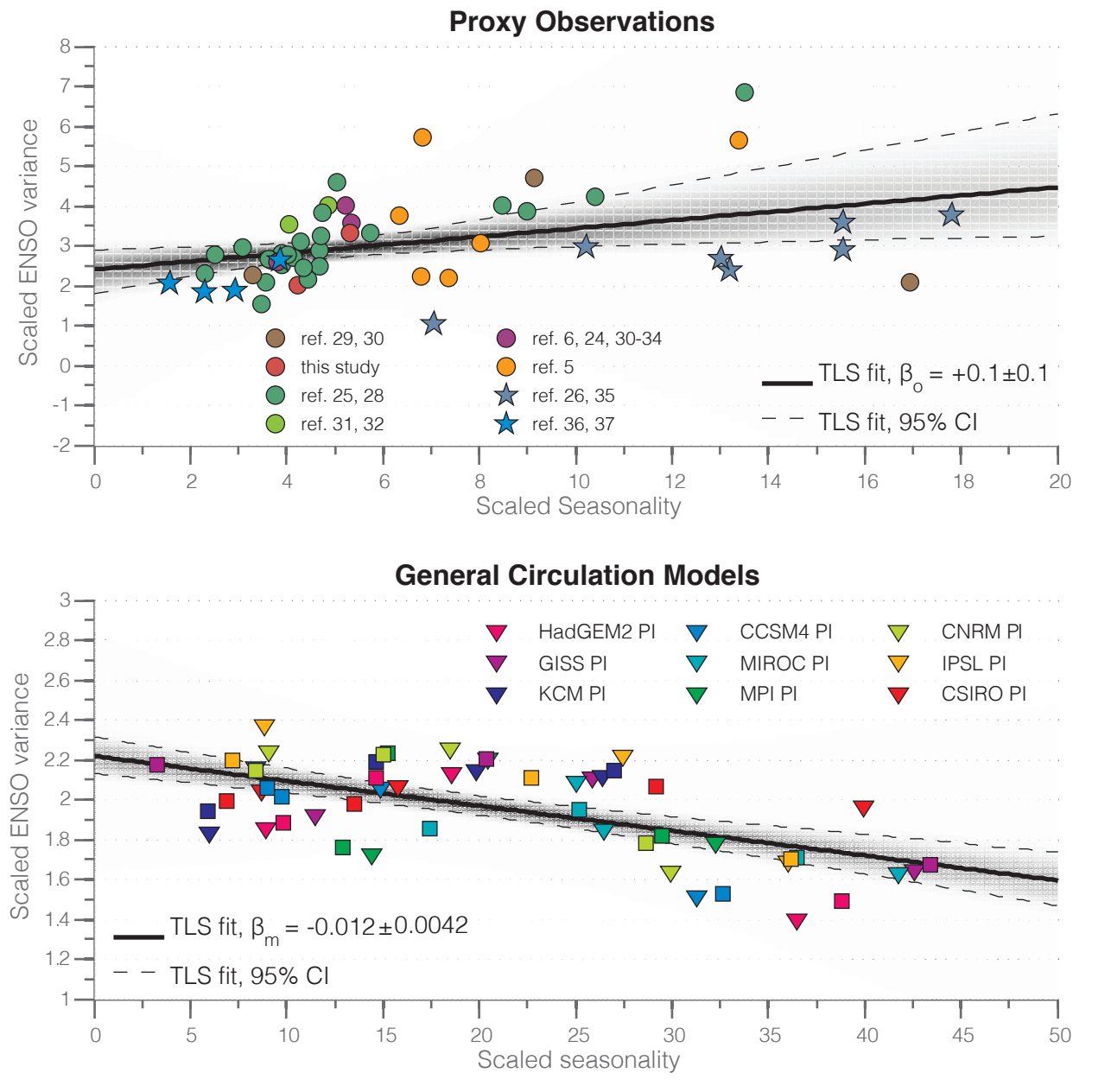
Proxy Observations
Scaled ENSO variance
Scaled Seasonality
ref. 29, 30
this study
ref. 25, 28
ref. 31, 32
ref. 6, 24, 30-34
ref. 5
ref. 26, 35
ref. 36, 37
TLS fit, β_o = +0.1±0.1
TLS fit, 95% CI
General Circulation Models
Scaled ENSO variance
Scaled seasonality
HadGEM2 PI
GISS PI
KCM PI
CCSM4 PI
MIROC PI
MPI PI
CNRM PI
IPSL PI
CSIRO PI
TLS fit, β_m = -0.012±0.0042
TLS fit, 95% CI